RSC Advances

PAPER

View Article Online
View Journal | View Issue

Cite this: *RSC Adv.*, 2020, **10**, 22645

Novel fabrication of PSSAMA_Na capped silver nanoparticle embedded sodium alginate membranes for pervaporative dehydration of bioethanol

Akshay S. Kulkarni,[a] Ashok M. Sajjan,*[a] Ashwini M,[b] Nagaraj R. Banapurmath,[c] Narasimha H. Ayachit[c] and Geeta G. Shirnalli[b]

Polystyrene-4-sulfonic acid co maleic acid sodium salt (PSSAMA_Na) capped silver nanoparticle (Ag_Np) embedded sodium alginate (Na-Alg) nanocomposite membranes have been developed to improve the pervaporation (PV) dehydration of bioethanol. The effect of PSSAMA_Na capped Ag_Nps on the micro-morphology, physicochemical properties and separation performance of the derived membranes was analyzed as a function of temperature at the azeotropic composition of the bioethanol–water mixture. WAXD analysis shows a decrease in crystalline domains with the increase in PSSAMA_Na capped Ag_Nps content and confirms the presence of Ag_Nps. DSC analysis demonstrated that the hydrophilic nature enhances as the PSSAMA_Na capped Ag_Nps content increases in the membrane matrix. Further, both total permeation flux and separation selectivity were increased with an increase in PSSAMA_Na capped Ag_Nps content. The results revealed that the membrane with 3 mass% of PSSAMA_Na capped Ag_Nps exhibited the highest permeation flux (13.40 × 10^{-2} kg m^{-2} h^{-1}) and separation selectivity (11 406) at 30 °C which indicate its better PV performance. The total permeation flux and permeation flux of water values were close to each other, which confirms that the membranes can be efficiently used to remove the water from azeotropic aqueous bioethanol.

Received 29th February 2020
Accepted 2nd June 2020

DOI: 10.1039/d0ra01951h

rsc.li/rsc-advances

1. Introduction

Ethanol is one of the most versatile natural solvents, and is miscible with water and many other organic solvents.[1,2] Bioethanol is also the principle fuel used as a petroleum substitute for road transport vehicles. It is the most well-known biofuel and is mostly a product of corn or sugarcane, and can be produced easily from biomass by fermentation.[3–5]

The azeotropic composition of aqueous bioethanol is 4% by mass. Bioethanol can be purified by distillation, adsorption, liquid–liquid extraction, and crystallization, which are often inefficient and uneconomic.[6,7] The shortcoming of these processes is that energy consumption is rather high, especially when the azeotropic composition is reached. Instead, the petrochemical industries are now considering pervaporation as a potential candidate to take up the increasing worldwide challenge of aromatics removal from gasoline, which remains one of the important issues concerning public health.

Pervaporation (PV), in its simplest type, is an association of lower energy consuming and an economical combination of membrane permeation and evaporation.[8,9] It is a membrane separation process, which uses a dense polymeric membrane for selective permeation of one or more components from a liquid mixture. In the process, the liquid mixture is kept in direct contact with one side of the membrane, and the permeated product (pervaporate) is removed in the form of vapor and condensed.

The productivity and success of the pervaporation process largely depend on the fabrication of suitable membranes with high permeability, good selectivity, and sufficient mechanical strength. Particularly, for the dehydration of alcohols, new membrane materials containing hydrophilic groups are usually preferred. In dehydration of alcohols through pervaporation, poly(vinyl alcohol),[10] sodium alginate,[11] chitosan[12,13] are the most preferred membrane materials, as they possess not only excellent hydrophilicity but also good film-forming ability.

Amid numerous polymeric materials for pervaporation, sodium alginate (Na-Alg) is natural and cost-effective polymer material proposed for alcohol–water separation considering the fact that it is hydrophilic and semi-crystalline in nature along with good membrane-forming ability, chemical-inertness, and thermal stability.[14]

However, owing to very high hydrophilic nature, Na-Alg membranes usually offer good permeation flux but less

[a]*Department of Chemistry, KLE Technological University, Hubballi 580031, India. E-mail: ashokmsajjan@gmail.com*

[b]*Department of Food and Industrial Microbiology, University of Agricultural Sciences, Dharwad 580 005, India*

[c]*Center for Material Science, KLE Technological University, Hubballi 580031, India*

separation selectivity as a consequence of too much swelling, which limits the performance of these membranes in PV separations. To overcome this, sodium alginate requires alteration to achieve better selectivity towards the water. Several modification methods such as cross-linking, grafting,[15] blending and incorporation of nanoparticles have been in use.[16]

Nano-materials have exceptional properties of strength, high surface area, thermal stability, optical activity, thermal and electrical conductivity, thereby resulting in many potential applications.[17–19] A literature survey reveals that by incorporating nano-materials in the membrane matrix, membrane properties like permeability, selectivity, and stability can be enhanced to achieve the excellent separation of bioethanol and water.[20–22]

In view of this, an attempt has been made to fabricate membranes for bioethanol dehydration by adding different fractions of polystyrene-4-sulfonic acid co maleic acid sodium salt (PSSAMA_Na) capped silver nanoparticles (Ag_Nps) in sodium alginate (Na-Alg) matrix. Increment in both separation selectivity and permeation flux at the same time is not commonly observed in PV due to the tradeoff phenomenon. Ag_Nps are not only hydrophilic property but also have anti bacterial properties which can contribute to the shelf life of the membranes. Materials like chitosan, methoxypolyethelene glycol, starch and even sodium alginate are used as stabilizer for Ag_Nps but the purpose of choosing PSSAMA_Na is that it has functional groups like $-COO^-$ and $-SO_3^-$ which contribute to enhance the hydrophilicity of the membranes. Further, $-SO_3^-$ groups also act as the capping agents to form ionic clusters with the Ag_Nps and $-COO^-$ groups cross-link with the –OH groups of Na-Alg.[23] This makes the membranes more selective towards water as well as contributes in the enhancement of permeation flux. To examine the changes in the peak intensities of the FTIR relating to the fraction of PSSAMA_Na capped Ag_Nps in the Na-Alg matrix, the FTIR spectra were recorded by keeping the amount of KBr and the membrane sample constant. To investigate the physicochemical properties of the resulting films thoroughly, they are characterized using WAXD, DSC, SEM, UTM and contact angle meter. Further, the effect of the content of PSSAMA_Na capped Ag_Nps and temperature on the pervaporation performance of the membranes for breaking the azeotropic point of the bioethanol–water mixture was tested.

2. Experimental

2.1 Materials

PSSAAMA_Na and Ag_Nps were procured from Sigma Aldrich Chemicals, USA. Na-Alg was purchased from S. D. Fine chemicals, India. Rectified bioethanol (96% ethanol and 4.0% water by mass) was procured from Godavari Biorefineries, Karnataka, India. Purchased chemicals were of reagent grade and were used without further purification. Double distilled water was used for the analysis.

2.2 Preparation of PSSAMA_Na capped Ag_Nps

2 mass% aqueous PSSAMA_Na solution was prepared by dissolving a certain amount of PSSAMA_Na in distilled water by constant stirring for 3 h. Then, 0.25 mass% of already sonicated Ag_Nps were put into aqueous PSSAMA_Na solution under constant stirring for about 2 h at 60 °C to obtain the PSSAMA_Na capped Ag_Nps suspension.[10]

2.3 Membrane fabrication

Na-Alg (3 gm) was dissolved in 105 mL of deaerated distilled water with constant stirring for about 24 h at room temperature. It was then filtered, and the resulting homogeneous solution was spread onto a clean glass plate with the aid of a casting knife in a dust-free atmosphere. It was allowed to dry at ambient temperature for about 2–3 days. The completely dried membrane was subsequently peeled-off and was designated as S-0.

To prepare PSSAMA_Na capped Ag_Nps embedded Na-Alg membrane, a known quantity of PSSAMA_Na capped Ag_Nps was added into the above prepared homogeneous Na-Alg solution. The resulting solution was stirred for 3 h at 60 °C, and then it was subjected to sonication at fixed frequency 38 kHz for about 30 minutes, so as to improve the dispersion of PSSAMA capped Ag_Nps in Na-Alg matrix. The solution thus obtained was poured onto a glass plate and the rest of the procedure was followed as similar to Membrane S-0. However, the amount of PSSAMA-capped Ag_Nps with respect to the sodium alginate was varied as 0.5, 1.0, 1.5, 2.0 and 3.0 mass%, and the resulting membranes were designated as S-0.5, S-1, S-1.5, S-2, and S-3 respectively.[14] An attempt was also made to incorporate higher amount of PSSAMA-capped Ag_Nps, but the membrane lost its properties. Therefore, we have restricted the addition of PSSAMA-capped Ag_Nps upto 3 mass%. The schematic representation of membrane fabrication is illustrated in Fig. 1.

2.4 Fourier transform infrared (FTIR) spectroscopy

Confirmation of reaction between PSSAMA_Na capped Ag_Nps and Na-Alg was done by FTIR Spectrometer (PerkinElmer spectrum, Singapore). The analysis was done using KBr method and the spectra were recorded in the range of 500–4000 cm^{-1}.

2.5 Wide-angle X-ray diffraction (WAXD)

Philips analytical X-ray diffractometer was used to obtain the X-ray diffractogram pattern of PSSAMA_Na capped Ag_Nps embedded Na-Alg membranes. For recognition of dried membrane samples having even thickness (~50 μm) were placed on the sample holder and at an angle 2θ and the analysis was done over a range of 5–80° at a speed of 8° min^{-1}.

2.6 Differential scanning calorimetry (DSC)

Differential scanning calorimeter (DSCQ 20, TA Instruments, Waters LLC, and New Castle, DE, USA) was used to study the crystalline and amorphous regions of the PSSAMA_Na capped Ag_Nps embedded Na-Alg membranes. Weight of samples ranging from 9 to 10 mg, which were subjected to heat from atmospheric temperature to 250 °C under nitrogen atmosphere at a heating rate of 10 °C min^{-1}.

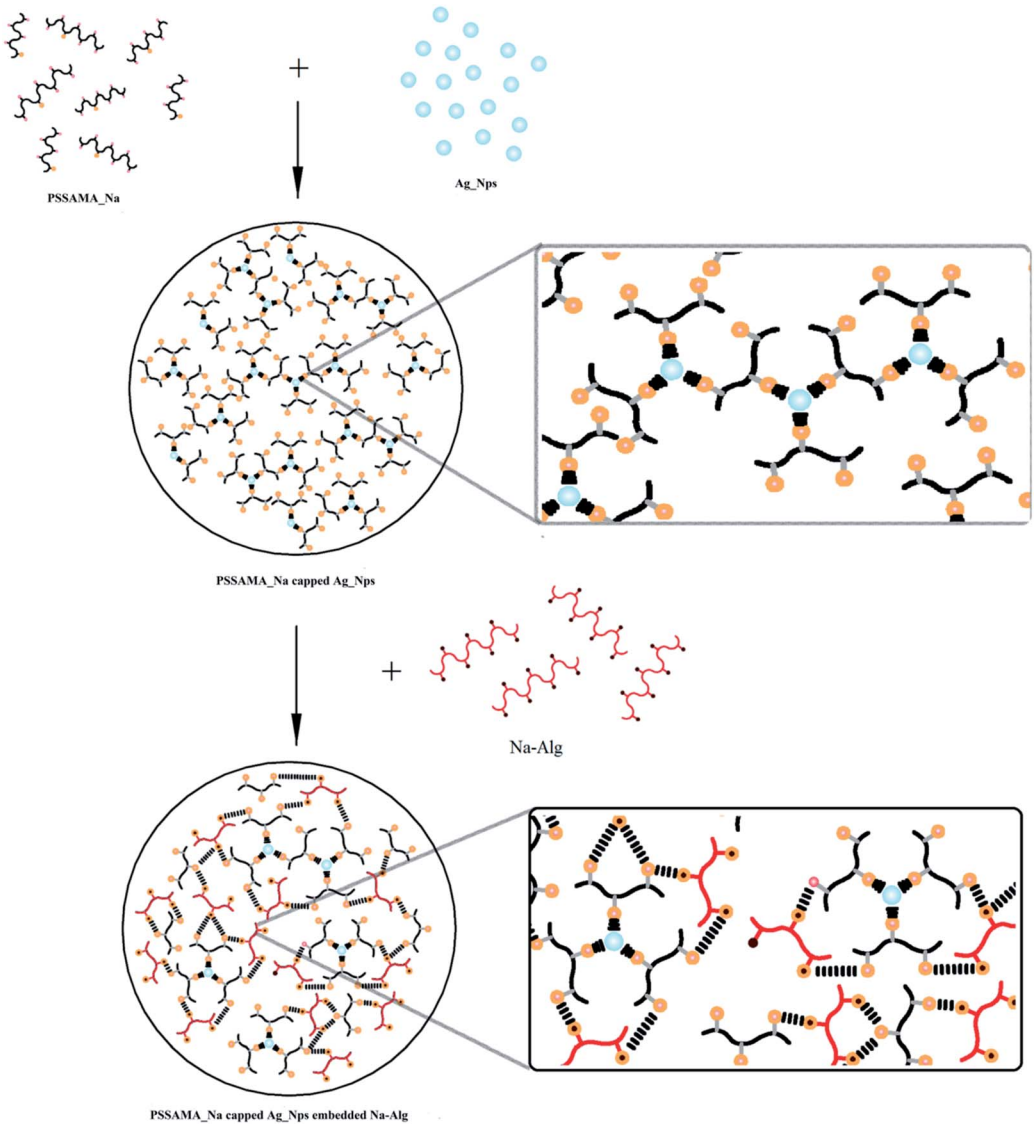

Fig. 1 Scheme for the fabrication of PSSAMA_Na capped Ag_Nps embedded Na-Alg membranes.

2.7 Scanning electron microscopy (SEM)

Analysis of Surface morphology of PSSAMA_Na capped Ag_Nps embedded Na-Alg membranes were carried out using a scanning electron microscope (JEOL, JSM-400 Å, Tokyo, Japan). Membrane samples were completely dried in order to take a photograph coated with a conductive layer (400 Å) of sputtered gold.

2.8 Contact angle measurements

The sessile droplet method was used to analyze static contact angles of water of PSSAMA_Na capped Ag_Nps embedded Na-Alg membranes with the help of a contact angle analyzer (Phoenix 300, South Korea) attached with a video camera. Each sample was tested for the contact angle of the water droplet with a time period of 10 seconds after placing it on the prepared membranes. With precision and accuracy provided by the software, the contact angle was measured with respect to the shape of the water droplet formed on the membranes.

2.9 Mechanical properties

The tensile strength and % elongation at break of the developed membranes were analyzed using the universal testing machine from Dak systems Inc. Membrane samples with a 25 × 50 mm dimension were considered for analysis. Three samples from each membrane were analyzed and the average results were considered.

2.10 Sorption analysis

The sorption experiments were done at 30 °C by taking the azeotropic composition of bioethanol and water mixture. First, the membranes were dried in an oven and then weighed. These membranes were then kept submerged in the ethanol–water mixture for 24 h in a closed container for equilibrium establishment. Further, the swollen membranes were carefully blotted and weighed. In order to find out the % degree of swelling, the following formula is used.

Fig. 2 Photographic image of the pervaporation apparatus: (A) front view: (1) permeate cold trap; (2) moisture cold trap; (3) control panel; (4) pervaporation cell; (5) vacuum pump; (6) vacuum control sensor. (B) Back view: (7) inlet and outlet of the feed tank; (8) feed tank; (9) circulation pump.

$$\text{DS } (\%) = \left(\frac{W_s - W_d}{W_d}\right) \times 100 \quad (1)$$

where W_s and W_d represent the weight of swollen and dry membranes respectively.

2.11 Pervaporation experiments

Sophisticated and specifically tailored pervaporation apparatus was employed for pervaporation experiments. The photograph of the PV unit is illustrated in Fig. 2. Heating vessel with a diameter of 300 mm with a volume of 4 liters used to fill the separating solution. The tank is completely sealed from the outer surrounding. Glass wool is used as an insulating material in the tank assembly. Heater with a power rating of 2.5 kW 230 V is used to maintain the required temperature inside the cylindrical tank. A heater is also equipped with a Pt-100 temperature sensor, which gives excellent accuracy at a broad temperature range. TC513BX is a sophisticated auto-tuning temperature controller or on/off the controller. Membrane holder with membrane surface area 15 cm^2 is made up of high-quality steel, which is chemically inert to the solvent as well as corrosion-resistant. Feed side with volume 4 liters is equipped with a circulating pump with controllable circulating speed. The vacuum of 31.325 kPa was kept in the permeate side using a vacuum pump which is equipped with a pressure gauge (PN2299 pressor sensor with display). The feed tank is also equipped with the stirrer to distribute the heat evenly throughout the liquid. After the equilibrium establishment of the membrane, the vacuum is applied, and the permeate vapors are condensed and collected in the cold trap at fixed intervals of time. Further, the permeation flux of the membrane was calculated after the measurement of the weight of the permeate using a digital microbalance. The composition of permeate was analyzed using KAFI smart Karl Fischer Titrator.

All the experiments were repeated three times and the average values were considered. However, the PV performance of the developed membranes was analyzed by calculating total permeation flux (J), separation selectivity (β) and pervaporation separation index (PSI) by using the following formulae.

$$J = \frac{W}{A \times t} \quad (2)$$

$$\beta = \frac{P_w/P_{ET}}{F_w/F_{ET}} \quad (3)$$

$$\text{PSI} = J(\beta - 1) \quad (4)$$

where W is the mass of permeate (kg); A, the effective membrane area (cm^2); t, the permeation time (h); P_w and P_{ET} are the mass percentages of water and bioethanol in permeate, respectively. F_w and F_{ET} are the respective mass percent of water and bioethanol in the feed.

Further, with the intention of getting a clear idea of the intrinsic properties of the membranes, the permeance (P_i/l) was evaluated using the following equation.

$$\frac{P_i}{l} = \frac{D_i K_i}{l} = \frac{j_i}{P_i^f - P_i^p} \quad (5)$$

where D_i and K_i are the diffusion and sorption coefficient of the i^{th} component respectively, P_i is the permeability of the i^{th} component, P_i^f and P_i^p are the vapor pressures of the i^{th} component in feed and permeate respectively and l is the membrane thickness. j_i is the molar flux of i^{th} component.

3. Results and discussions

3.1 Fourier transform infrared spectroscopy (FTIR)

Fig. 3 exhibits the FTIR spectra of sodium alginate (Na-Alg) and its PSSAMA_Na capped Ag_Nps membranes.

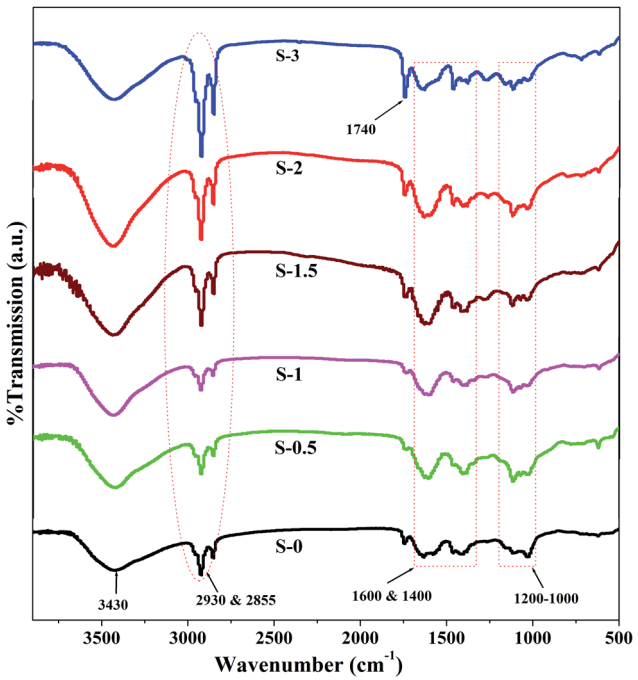

Fig. 3 FTIR spectra of Na-Alg and its PSSAMA_Na capped Ag_Nps embedded membranes: pure Na-Alg; (S-0) 0 mass%; (S-0.5) 0.5 mass%; (S-1) 1 mass%; (S-1.5) 1.5 mass%; (S-2) 2 mass%; (S-3) 3 mass% of PSSAMA_Na capped Ag_Nps.

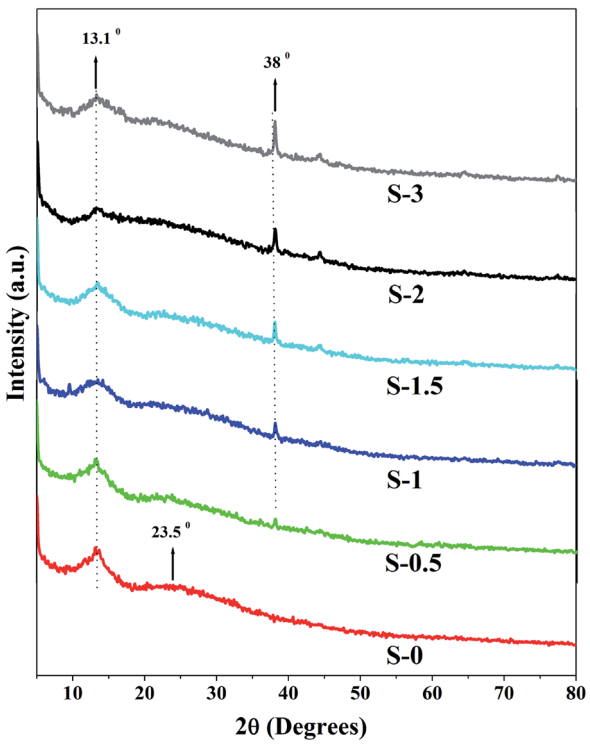

Fig. 4 Wide-angle X-ray diffraction patterns of Na-Alg and its PSSAMA_Na capped Ag_Nps embedded membranes: pure Na-Alg; (S-0) 0 mass%; (S-0.5) 0.5 mass%; (S-1) 1 mass%; (S-1.5) 1.5 mass%; (S-2) 2 mass%; (S-3) 3 mass% of PSSAMA_Na capped Ag_Nps.

In pure Na-Alg, a characteristic broad band visible at 3430 cm^{-1} corresponds to –OH stretching vibrations. Further, the bands for asymmetric and symmetric –C=O stretching appeared around 1600 cm^{-1} and 1400 cm^{-1} respectively. Similarly, multiple peaks appeared in the range of 1000 cm^{-1} to 1200 cm^{-1} and the peaks at 2855 cm^{-1} and 2930 cm^{-1} correspond to –CO and –CH stretching respectively.[24] Further, the intensity of the peak appearing around 1740 cm^{-1} corresponding to ester formation between $-COO^-$ groups of PSSAMA_Na and –OH groups of Na-Alg was gradually increased as the content of PSSAMA_Na increased in the membrane matrix (S-1 to S-3). The new peaks appeared at around 1040 cm^{-1} and 1130 cm^{-1} in PSSAMA_Na capped Ag_Nps embedded membranes correspond to symmetric and asymmetric stretching of S=O groups. Similarly, two peaks appearing at 2855 cm^{-1} and 2930 cm^{-1} correspond to $-SP_3$ hybridized –CH stretching. The intensity of these peaks was also gradually increased as the PSSAMA_Na concentration increased, owing to the increase in the number of –CH groups. Further, the peak intensity of the broad band appeared around 3430 cm^{-1} was enhanced not only due to enhanced hydrogen bonding but also due to the increased cross-linking.[25] Based on this spectral evidence, it can be concluded that the PSSAMA_Na capped Ag_Nps enhanced cross-linking as well as the hydrophilic nature of the membranes.

3.2 Wide-angle X-ray diffraction (WAXD)

WAXD plays a vital role in analyzing the degree of crystallinity and modifications in the structure of the developed membranes. Fig. 4 illustrates the WAXD patterns of the developed membranes.

In the patterns, the Na-Alg membrane demonstrated typical diffraction peaks at $2\theta = 13.1°$ and 23.5° which are assigned to crystalline and amorphous regions respectively.[26] However, the intensity of these peaks gradually decreased as the content of PSSAMA_Na capped Ag_Nps increased in the membrane matrix. This is due to the ionic clusters formed by Ag_Nps and $-SO_3^-$ groups of PSSAMA_Na which disordered the polymer chain arrangement and reduced the formation of crystalline regions in the membrane. Because of which the amorphous domain was enhanced in the membrane. Further, a new peak appeared at $2\theta = 38°$ correspond to the presence of Ag_Nps.[27] However, the peak intensity was gradually enhanced as the PSSAMA_Na capped Ag_Nps content was increased in the membrane matrix which proves the increased content of Ag_Nps which leads to the enhanced hydrophilicity of the membrane.[25]

3.3 Differential scanning calorimetry (DSC)

Fig. 5 illustrates the thermograms of the developed membranes.

From the figure, it is noticed that the Na_Alg membrane exhibits an endothermic peak (T_g) at 84 °C. However, from S-0.5 to S-3, the endothermic peak gradually enhanced in terms of area under the curve as well as shifted slightly to a higher temperature as the content of PSSMA_Na capped Ag_Nps increased in the membrane matrix. This indicates that the stabilized Ag_Nps and polar groups present in the membrane matrix (–OH, $-SO_3^-$ and $-COO^-$) increased hydrophilicity of the

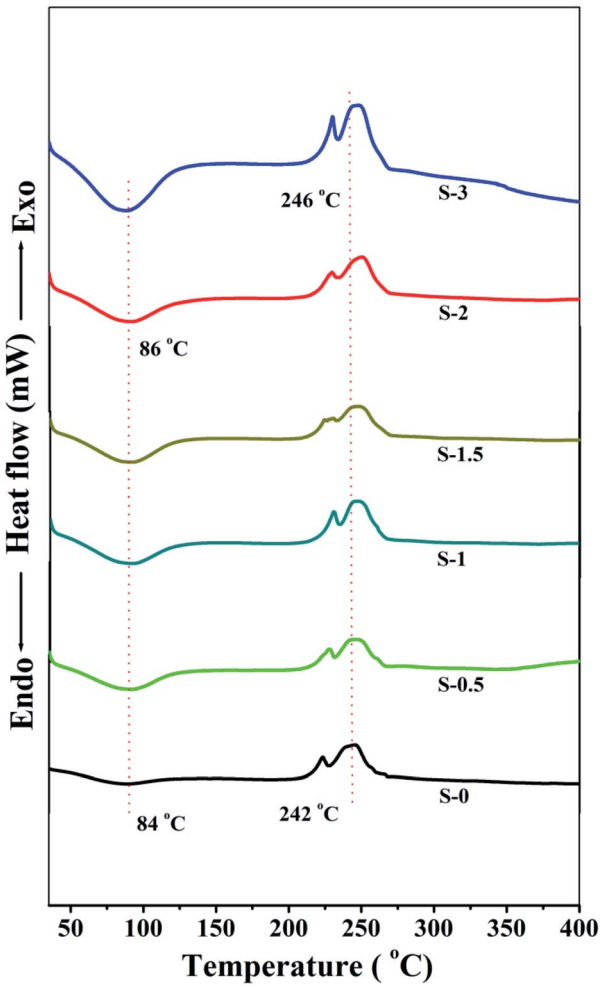

Fig. 5 DSC thermograms of Na-Alg and its PSSAMA_Na capped Ag_Nps embedded membranes: pure Na-Alg; (S-0) 0 mass%; (S-0.5) 0.5 mass%; (S-1) 1 mass%; (S-1.5) 1.5 mass%; (S-2) 2 mass%; (S-3) 3 mass% of PSSAMA_Na capped Ag_Nps.

membranes and also suppressed the crystalline domains in the membranes. This leads to the higher water holding capacity of the membranes. Thus it can be said that the transport of molecules through the membranes is dominated by amorphous phase and hence the membrane with the highest content of PSSAMA_Na capped Ag_Nps demonstrated the highest permeation flux.

3.4 Scanning electron microscopy (SEM)

Fig. 6 demonstrates the SEM photographs (surface views) of the developed membranes.

From the micrographs, it was clear that there was no significant increase of the bright regions in the SEM images from membrane S-0.5 to S-3. This may provide a piece of evidence for the successful capping of Ag_Nps. It was further noticed that the PSSAMA_Na capped Ag_Nps were distributed evenly throughout the membrane matrix with no apparent clustering. Therefore, this ascertains that the developed membranes are homogenous and free from defects.

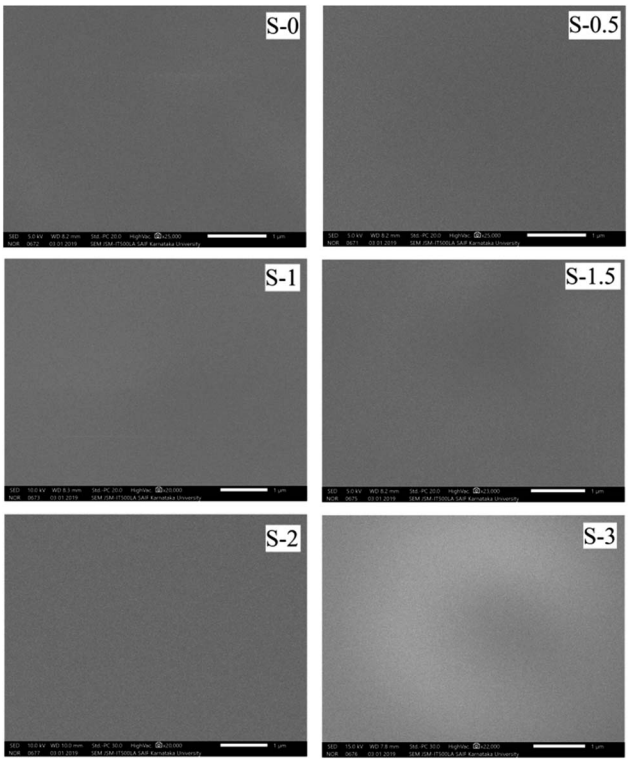

Fig. 6 SEM micrographs of Na-Alg and its PSSAMA_Na capped Ag_Nps embedded membranes: pure Na-Alg; (S-0) 0 mass%; (S-0.5) 0.5 mass%; (S-1) 1 mass%; (S-1.5) 1.5 mass%; (S-2) 2 mass%; (S-3) 3 mass% of PSSAMA_Na capped Ag_Nps.

3.5 Contact angle measurements

Contact angle values play an important role in analyzing the hydrophilicity of the membrane surface which influences the permeation flux of the membrane. The contact angle values of

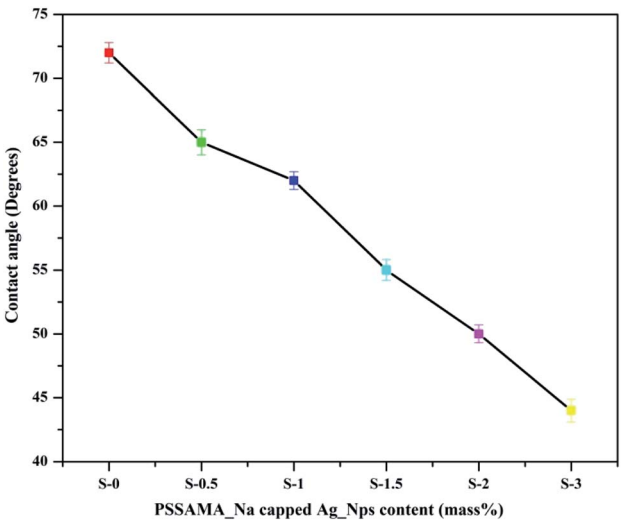

Fig. 7 Contact angles of Na-Alg and its PSSAMA_Na capped Ag_Nps embedded membranes: pure Na-Alg; (S-0) 0 mass%; (S-0.5) 0.5 mass%; (S-1) 1 mass%; (S-1.5) 1.5 mass%; (S-2) 2 mass%; (S-3) 3 mass% of PSSAMA_Na capped Ag_Nps.

Table 1 The mechanical properties of the developed membranes

Membrane	Tensile strength (MPa)	% elongation at break
S-0	43.88 ± 3.24	7.49 ± 1.24
S-0.5	41.91 ± 2.19	5.86 ± 2.17
S-1	34.52 ± 3.00	5.66 ± 2.78
S-1.5	30.53 ± 3.23	4.37 ± 2.96
S-2	29.26 ± 3.21	3.25 ± 1.98
S-3	22.04 ± 2.68	2.83 ± 2.01

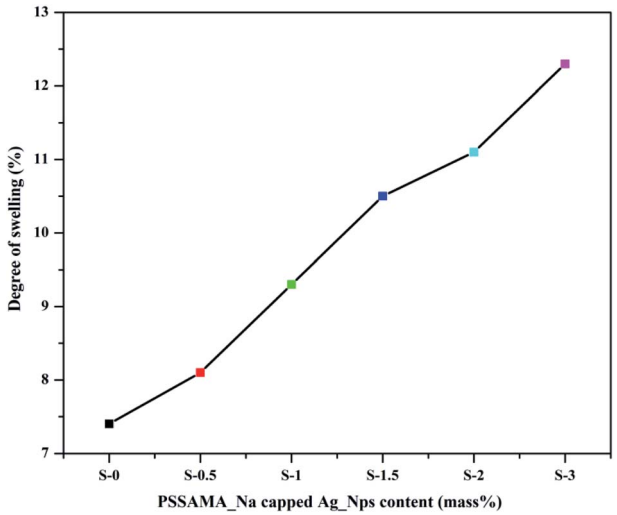

Fig. 8 Effect PSSAMA_Na capped Ag_Nps content on membrane sorption.

the developed membranes are represented in Fig. 7. The contact angle of 72° was observed for the pure Na_Alg membrane. After the incorporation of PSSAMA_Na capped Ag_Nps in the Na-Alg matrix, the contact angle value was decreased systematically from 65° to 44°. This is due to evenly dispersed ionic clusters in the Na-Alg matrix disturbs the chain arrangement which leads to the increased amorphous nature as well as the hydrophilicity of the membranes. Moreover, the number of polar groups (–OH, $-SO_3^-$ and $-COO^-$) present in the membrane matrix also contribute to the increased hydrophilicity.

3.6 Mechanical properties

Tensile strength and elongation at break of the membrane describe the mechanical strength of the membranes and their suitability towards the pervaporation.[28] The effect of increased content of the Ag_Nps on the strength and percentage elongation at break of the membranes were analyzed and illustrated in Table 1. From the obtained values, it could be observed that the tensile strength of the membranes decreased from 43.8 to 22.0 MPa as the PSSAMA_Na capped Ag_Nps content increased in the membrane. This was expected because the addition of PSSAMA_Na capped Ag_Nps content in the Na-Alg matrix might increase hydrophilic susceptibility and decrease the entanglement degree which leads to poor mechanical strength. The capping of Ag_Nps will act as a stabilizer for Ag_Nps which will prevent the aggregation in the bulk or on the surface which is beneficial for the membrane. But it will lead to the decrement in the strength of the membrane. Despite this, the membrane can be efficiently used for the pervaporation separation of bioethanol.

3.7 Sorption analysis

Membrane sorption plays a crucial role in organic dehydrations under the potential chemical gradient. The degree of swelling will help in the analysis of selective permeation of molecules, which is vital in the PV process. The plots of % degree of swelling *versus* concentration of PSSAMA_Na capped Ag_Nps at 30 °C is shown in Fig. 8. Membrane sorption was observed rising as the content of PSSAMA_Na capped Ag_Nps was increased in the membrane matrix. This was obvious as the interactions between the water molecules and the membranes were increased owing to the presence of Ag_Nps, –OH, $-SO_3^-$ and $-COO^-$ groups in the membrane matrix. S-3 exhibited the highest degree of swelling (12.3%) due to the highest concentration of PSSAMA_Na capped Ag_Nps which enhances interactions between the water molecules and the membrane.

3.8 Effects of PSSAMA_Na capped Ag_Nps on the pervaporation

Table 2 illustrates the effects of PSSAMA_Na capped Ag_Nps on the PV performance of the developed membranes. From the data, it was clearly noticed that as the content of PSSAMA_Na capped Ag_Nps was enhanced, separation selectivity, total permeation flux and permeance were increased. These results are in accordance with the data of the sorption study and contact angle. The increase observed in the permeation flux was almost linear with S-3 showing the value 0.1340 kg m^{-2} h^{-1} at

Table 2 Permeation flux, separation selectivity and permeance data of the developed membranes at various temperatures[a]

Membrane	Temperature (°C)	$J \times 10^{-2}$ (kg m^{-2} h^{-1})	β	P_i/l (GPU)
S-0	30	10.47	3014	2094
	40	11.40	2401	2280
	50	13.20	2219	2640
S-0.5	30	11.47	3613	2294
	40	12.07	2976	2414
	50	13.67	2425	2734
S-1	30	12.27	5558	2454
	40	12.80	4044	2560
	50	14.07	3559	2814
S-1.5	30	12.73	7250	2546
	40	13.27	4875	2654
	50	14.33	3977	2866
S-2	30	12.93	8549	2586
	40	13.40	5830	2680
	50	14.60	4262	2920
S-3	30	13.40	11 406	2680
	40	14.00	6293	2800
	50	15.13	4875	3026

[a] GPU = gas permeation unit = 10^{-6} cm^3 (STP)/cm^2/s/cm Hg.

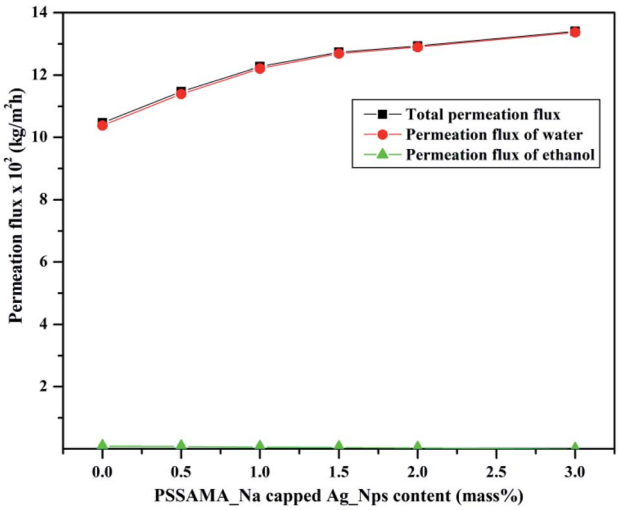

Fig. 9 Deviation in total permeation flux and permeation fluxes of water and ethanol at 30 °C.

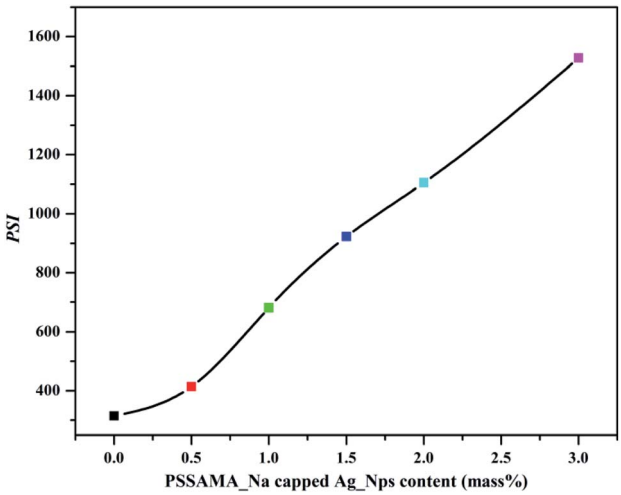

Fig. 10 Effect of concentrations of PSSAMA_Na capped Ag_Nps on PSI at 30 °C.

30 °C. This is expected due to the presence of PSSAMA_Na capped Ag_Nps which enhances the hydrophilicity of the membrane. Ag_Nps present in the membrane enhanced hydrophilicity and decreased crystalline regions of the membrane, which led to the higher interactions between the membrane and the water.

Increment in both separation selectivity and permeation flux at the same time is not commonly observed in PV due to the tradeoff phenomenon. Incorporation of fillers or cross-linking typically directs to the enhanced membrane density which leads to the lower permeation flux and higher separation selectivity. However, in this research study, both separation selectivity and permeation flux were simultaneously increased with an increase in the content of PSSAMA_Na capped Ag_Nps in the membrane matrix. This is because the ionic groups like $-COO^-$ and $-SO_3^-$ present in PSSAMA_Na and Ag_Nps will contribute to the better permeation flux and the cross-linking reactions between PSSAMA_Na and Na-Alg contributed to elevated separation selectivity.

Fig. 9 shows the plots of total permeation flux and permeation fluxes of water and ethanol considered as a function of the content of PSSAMA_Na capped Ag_Nps. From the figure, it can be noticed that the curve of permeation flux of water and the curve of total permeation flux is almost merging, whereas the permeation flux of ethanol is almost suppressed. This provides proof of the hydrophilic nature of membranes.

3.9 Effect of PSSAMA_Na capped Ag_Nps on the pervaporation separation index (PSI)

Pervaporation separation index can be employed as a fundamental parameter to analyze the separation efficiency of the membrane as it depends on both permeation flux and separation selectivity. The plot of PSI values at various concentrations of PSSAMA_Na capped Ag_Nps at 30 °C is shown in Fig. 10. From the figure, it was observed that the PSI values are increasing systematically as the concentration of PSSAMA_Na capped Ag_Nps was increased. This was obvious as the permeation flux and separation selectivity were increasing simultaneously as the content of PSSAMA_Na capped Ag_Nps increased in the membrane matrix. Membrane S-3 exhibited the highest PSI value (1528) amongst the developed membranes, which indicate that it demonstrated better PV performance.

3.10 Effect of temperature on membrane performance

Table 2 represents the temperature effect on the PV performance of the developed membranes. From the table, it was noticed that the permeation flux was enhanced for all the membranes as the temperature was increased. Firstly, as a result of the increment in the temperature, a pressure difference is created between the upstream and the downstream ends of the membrane which in turn acts as a driving force for transport of the molecules. Secondly, due to the increase in the temperature, the free volume of the polymer matrix as well as thermal motion in polymer segments increase. However, the second reason can be disqualified as the experiments were conducted well below the glass transition temperature of the polymer. Therefore, the driving force is considered as a major influence in the enhancement of permeation flux along with the decrement in separation selectivity.

3.11 Comparison of PV performance with the literature

Table 3 represents the comparison between the obtained PV results and the PV results in the literature for the separation of aqueous ethanol at the azeotropic point using different membranes. From the literature it can be observed that, the separation selectivity of the developed membranes is far more higher compared to the other membranes. Few membranes namely polyacrylonitrile–polyvinylpyrrolidone, Teflon-*g*-polyvinylpyrrolidone, all Nafion membranes and all PVA/GA membranes exhibit higher permeation flux but this was achieved by sacrificing the separation selectivity. Moreover, all these membranes exhibited higher permeation flux values at

Table 3 Comparative study of PV performance of different membranes reported in the literature for dehydration of ethanol at azeotropic point[a]

Membrane	Temperature (°C)	Separation selectivity	Permeation flux (g m^{-2} h^{-1})	Ref.
Nafion-H^+	70	2.5	5000	29
Polyacrylonitrile–polyvinylpyrrolidone	20	3.2	2200	30
Polystyrene	40	101	5	31
Poly(vinyl chloride)	40	63	3	32
Alginic acid	40	8.8	48	33
Chitosan	40	2208	4	34
Chitosan acetate salt	40	2556	2	35
Chitosan/GA	40	202	7	35
Cationic PVA/GA	40	709	89	36
Anionic PVA/GA	40	837	86	36
PVA/GA	40	335	189	36
PVA/GA acrylic acid	40	14	135	37
Unmodified PVA	40	15	91	37
Nafion-Na^+	70	5.0	500	29
Nafion-K^+	70	9.8	200	29
Cellulose acetate	60	5.9	200	38
Teflon-*g*-polyvinylpyrrolidone	25	2.9	2200	38
Na-Alg	30	3014	105	Present work
Na-Alg/0.5% Ag_Nps–PSSAMA_Na	30	3613	115	Present work
Na-Alg/1.0% Ag_Nps PSSAMA_Na	30	5558	123	Present work
Na-Alg/1.5% Ag_Nps–PSSAMA_Na	30	7250	127	Present work
Na-Alg/2.0% Ag_Nps–PSSAMA_Na	30	8549	129	Present work
Na-Alg/3.0% Ag_Nps–PSSAMA_Na	30	11 406	134	Present work

[a] Na-Alg: sodium alginate, PSSAMA_Na: polystyrene-4-sulfonic acid co maleic acid sodium salt, GA: glutaraldehyde, PVA: poly(vinyl alcohol), Ag_Nps: silver nanoparticles.

Table 4 Comparative study of PV performance of Na-Alg based membranes reported in the literature for dehydration of ethanol[a]

Membrane	Temp. (°C)	Mass% of water in the feed	Permeation flux (kg m^{-2} h^{-1})	Separation selectivity	Ref.
GA–Na-Alg	60	10.0	0.3	1000	39
GA–Na-Alg/CS	60	10.0	0.3	200	39
Na-Alg–H_3PO_4	30	5.2	0.24	2182	40
CS/Na-Alg	30	13.5	0.22	436	40
6% P-HPA–Na-Alg	30	4.0	0.17	59 976	41
6% P-HPA–Na-Alg	30	10.0	0.57	14 991	41
Two-ply composite Na-Alg/CS	30	5.0	0.07	1110	41
2.5% zeolite–Na-Alg	30	10.0	0.052	256	42
5% zeolite–Na-Alg	30	10.0	0.095	540	42
7.5% zeolite–Na-Alg	30	10.0	0.112	773	42
10% zeolite–Na-Alg	30	10.0	0.132	1598	42
CL/Ca^{2+}–Na-Alg	30	10.0	0.068	1175	42
P-PVP/Na-Alg	30	10.0	0.09	364	43
1% Al-MCM-41/Na-Alg	30	10.0	0.027	35	44
5% Al-MCM-41/Na-Alg	30	10.0	0.060	377	44
8% Al-MCM-41/Na-Alg	30	10.0	0.092	949	44
20% Al-MCM-41/Na-Alg	30	10.0	0.129	1089	44
Na-Alg	30	4.0	0.105	3014	Present work
Na-Alg/0.5% Ag_Nps–PSSAMA_Na	30	4.0	0.115	3613	Present work
Na-Alg/1.0% Ag_Nps PSSAMA_Na	30	4.0	0.123	5558	Present work
Na-Alg/1.5% Ag_Nps–PSSAMA_Na	30	4.0	0.127	7250	Present work
Na-Alg/2.0% Ag_Nps–PSSAMA_Na	30	4.0	0.129	8549	Present work
Na-Alg/3.0% Ag_Nps–PSSAMA_Na	30	4.0	0.134	11 406	Present work

[a] Na-Alg: sodium alginate, PSSAMA_Na: polystyrene-4-sulfonic acid co maleic acid sodium salt, CS: chitosan, GA: glutaraldehyde, P-HPA: preyssler heteropolyacid, P-PVP: phosporylated poly(vinyl pyrrolidone), Al-MCM-41: aluminum-containing mesoporous silica, Ag_Nps: silver nano particles, CL: cellulose.

elevated temperatures except polyacrylonitrile–polyvinylpyrrolidone and Teflon-*g*-polyvinylpyrrolidone. The developed membranes exhibited excellent separation selectivity and moderately good permeation flux at ambient temperatures.

Table 4 represents the comparison between the obtained PV results and the PV results in the literature for the separation of aqueous ethanol using Na-Alg membranes. From the literature it can be observed that, the separation selectivity of the developed membranes is far more higher compared to the other membranes except 6% P-HPA–Na-Alg membranes. The higher PV performance of 6% P-HPA–Na-Alg membranes was due to the discrete structure of HPAs comprising the heteropolyanions and the mobile solvated protons. All the other membranes reported in the table are exhibiting higher permeation flux in comparison with the permeation flux of the developed membranes. However, this was achieved by sacrificing the separation selectivity and due to more content of water in the feed.

4. Conclusion

PSSAMA_Na capped Ag_Nps embedded Na-Alg membranes were fabricated and analyzed for separation of the azeotropic aqueous bioethanol at various temperatures. Membranes demonstrated reasonably good PV performance. FTIR confirmed the cross-linking reaction between Na-Alg and PSSAMA_Na. WAXD shows a decrease in crystalline domains with an increase in PSSAMA_Na capped Ag_Nps content as well as confirm the presence of Ag_Nps. Contact angle and sorption analysis data prove the enhancement in the hydrophilicity as the content of PSSAMA_Na capped Ag_Nps was increased. DSC illustrated that, as the PSSAMA_Na capped Ag_Nps content increased in the membrane matrix, the area under the curve is enhanced as well as shifted slightly to a higher temperature. This indicates that the stabilized Ag_Nps and polar groups present in the membrane matrix (–OH, $-SO_3^-$ and $-COO^-$) increased hydrophilicity of the developed membranes. The compatibility of the chemicals and uniform distribution of the PSSAMA_Na capped Ag_Nps is confirmed by SEM images. Membrane S-3 exhibited the tensile strength of 22.04 MPa which is good enough to carry out the PV experiments at various temperatures. Developed membranes exhibited an anti tradeoff phenomenon that is both separation selectivity and permeation flux were increased simultaneously with an increase in the content of PSSAMA_Na capped Ag_Nps in the membrane matrix. Among the PSSAMA_Na capped Ag_Nps embedded membranes, the Membrane containing 3 mass% of PSSAMA_Na capped Ag_Nps demonstrated the highest separation selectivity of 11 406 with a permeation flux of 13.40×10^{-2} kg m^{-2} h^{-1} at 30 °C for azeotropic aqueous bioethanol.

Nomenclature

M_w	Molecular weight
A	Effective membrane area
DS	Degree of swelling (%)
ET	Ethanol
J	Total flux
J_o	Pre-exponential factor for permeation
PSI	Pervaporation separation index
P and F	Mass percent of permeate and feed
T	Permeation time (h)
T	Temperature (K)
W	Mass of permeate
W_s and W_d	Mass of the swollen and dry membranes

Conflicts of interest

There are no conflicts to declare.

Acknowledgements

Authors gratefully acknowledge financial support from Vision Group on Science and Technology, Karnataka, India (No. K-FIST(L2)/2016-17/GRD-540/2017-18/103/3).

References

1 J. Y. Park, I. H. Lee and G. N. Bea, *J. Ind. Eng. Chem.*, 2008, **14**, 707–713.
2 T. Ding and J. Zhu, *Mater. Sci. Eng. B*, 2003, **100**, 307–313.
3 Y. Lin and S. Tanaka, *Appl. Microbiol. Biotechnol.*, 2006, **69**, 627–642.
4 G. Najafpour, H. Younes and K. S. K. Ismail, *Bioresour. Technol.*, 2004, **92**, 251–260.
5 C. K. Yamakawa, E. C. Rivera, H. Kwond, W. E. H. Agudelo, M. B. W. Saad, J. Leal, C. E. V. Rossell, A. Bonomi and R. M. Filho, *Biochemical Engineering Chemistry*, 2019, **147**, 1–10.
6 L. M. Vane, *J. Chem. Technol. Biotechnol.*, 2005, **80**, 603–629.
7 T. M. Boudreau and G. A. Hill, *Process Biochem.*, 2006, **41**, 980–983.
8 S. G. Adoor, S. D. Bhat, D. D. Dionysiou, M. N. Nadagouda and T. M. Aminabhavi, *RSC Adv.*, 2014, **4**, 52571–52582.
9 C. Ji, S. Xue and Z. Xu, *ACS Appl. Mater. Interfaces*, 2016, **8**, 27243–27253.
10 F. Peng, F. Pan, H. Sun, L. Lu and Z. Jiang, *J. Membr. Sci.*, 2007, **300**, 13–19.
11 M. Wang, R. Xing, H. Wu, F. Pan, J. Zhang, H. Ding and Z. Jiang, *J. Membr. Sci.*, 2017, **538**, 86–95.
12 G. Dudek and R. Turczyn, *RSC Adv.*, 2018, **8**, 39567–39578.
13 D. Unlu and N. D. Hilmioglu, *J. Membr. Sci.*, 2018, **559**, 138–147.
14 A. M. Sajjan, B. K. Jeevan Kumar, A. A. Kittur and M. Y. Kariduraganavar, *J. Membr. Sci.*, 2013, **425–426**, 77–88.
15 A. S. Kulkarni, S. M. Badi, A. M. Sajjan, N. R. Banapurmath, M. Y. Karidurganavar and A. S. Shettar, *Chem. Data Collect.*, 2019, **22**, 100245.
16 Y. K. Ong, G. M. Shi, N. L. Le, Y. P. Tang, J. Zuo, S. P. Nunes and T. S. Chung, *Prog. Polym. Sci.*, 2016, **57**, 1–31.
17 A. M. Sajjan, N. R. Banapurmath, N. M. Shivayyanavar, A. S. Kulkarni and A. S. Shettar, *IOP Conf. Ser.: Mater. Sci. Eng.*, 2018, **376**, 012073.

18 S. Claes, P. Vandezande, S. Mullens, R. Leysen, K. De Sitter, A. Andersson, F. H. J. Maurer, H. Van den Rul, R. Peeters and M. K. Van Bael, *J. Membr. Sci.*, 2010, **351**, 160–167.
19 L. Diestel, H. Bux, D. Wachsmuth and J. Caro, *Microporous Mesoporous Mater.*, 2012, **164**, 288–293.
20 H. Azimi, F. Tezel and J. Thibault, *J. Chem. Technol. Biotechnol.*, 2017, **92**, 2901–2911.
21 L. Gong, L. Zhang, N. Wang, J. Li, S. Ji, H. Guo, G. Zhang and Z. Zhang, *Sep. Purif. Technol.*, 2014, **122**, 32–40.
22 Y. Huang, P. Zhang, J. Fu, Y. Zhou, X. Huang and X. Tang, *J. Membr. Sci.*, 2009, **339**, 85–92.
23 L. Guo, W. Yuan, Z. Lu and C. M. Li, *Colloids Surf., A*, 2013, **439**, 69–83.
24 T. Zhu, Y. Luo, Y. Lin, Q. Li, P. Yu and M. Zeng, *Sep. Purif. Technol.*, 2010, **74**, 242–252.
25 H. G. Premakshi, A. M. Sajjan, A. A. Kittur and M. Y. Kariduraganavar, *J. Appl. Polym. Sci.*, 2014, **132**, 41248.
26 P. S. Rachipudi, A. A. Kittur, A. M. Sajjan, R. R. Kamble and M. Y. Kariduraganavar, *Chem. Eng. Sci.*, 2013, **94**, 84–92.
27 K. Anandalakshmi, J. Venugobal and V. Ramasamy, *Appl. Nanosci.*, 2016, **6**, 399–408.
28 A. M. Sajjan, M. L. Naik, A. S. Kulkarni, U. Rudgi, M. Ashwini, G. G. Shirnalli, A. Sharanappa and P. B. Kalahal, *Chem. Data Collect.*, 2020, **26**, 100338.
29 T. Ishikawa, *Kemikaru Enjiniyaringu*, 1984, **29**, 19–25.
30 Q. T. Nguyen, L. Le Blanc and J. Neel, *J. Membr. Sci.*, 1985, **22**, 245–255.
31 T. Uragami and T. Morikawa, *Macromol. Chem. Phys.*, 1989, **190**, 399–404.
32 T. Uragami, T. Morikawa and H. Okuno, *Polymer*, 1989, **30**, 1117–1122.
33 T. Uragami and M. Saito, *Sep. Sci. Technol.*, 1989, **24**, 541–554.
34 T. Uragami, H. Matsugi and T. Miyata, *Macromolecules*, 2005, **38**, 8440–8446.
35 T. Uragami and K. Takigawa, *Polymer*, 1990, **31**, 668–672.
36 V. S. Praptowidodo, *J. Mol. Struct.*, 2005, **739**, 207–212.
37 M. Rafik, A. Mas, M.-F. Guimon, C. Guimon, A. Elharfi and F. Schué, *Polym. Int.*, 2003, **52**, 1222–1229.
38 B. Bolto, M. Hoang and Z. Xie, *Chem. Eng. Process.*, 2011, **50**, 227–235.
39 P. Shao and R. Y. M. Huang, *J. Membr. Sci.*, 2007, **287**, 162–179.
40 S. Kalyani, B. Smitha, S. Sridhar and A. Krishnaiah, *Desalination*, 2008, **229**, 68–81.
41 V. T. Magalad, A. R. Supale, S. P. Maradur, G. S. Gokavi and T. M. Aminabhavi, *Chem. Eng. J.*, 2010, **159**, 75–83.
42 S. G. Adoor, L. S. Manjeshwar, S. D. Bhat and T. M. Aminabhavi, *J. Membr. Sci.*, 2008, **318**, 233–246.
43 S. Kalyani, B. Smitha, S. Sridhar and A. Krishnaiah, *Ind. Eng. Chem. Res.*, 2006, **45**, 9088–9095.
44 M. B. Patil, R. S. Veerapur, S. A. Patil, C. D. Madhusoodana and T. M. Aminabhavi, *Sep. Purif. Technol.*, 2007, **54**, 34–43.